Dalton Transactions

PAPER

View Article Online
View Journal | View Issue

Cite this: *Dalton Trans.*, 2016, **45**, 1185

Synthesis and characterization of metastable β-Ag_2WO_4: an experimental and theoretical approach†

Pablo S. Lemos,[a] A. Altomare,[b] A. F. Gouveia,[a] I. C. Nogueira,[c] L. Gracia,[d,e] R. Llusar,[e] J. Andrés,*[e] E. Longo[a,d] and Laécio S. Cavalcante[f]

Metastable silver tungstate (β-Ag_2WO_4) has attracted much attention lately because of its many potential applications. However, the synthesis of metastable phases of inorganic compounds is challenging because of the ease of transformation to the stable phase. We have overcome this challenge and have successfully synthesized β-Ag_2WO_4 microcrystals using a dropwise precipitation (DP) method in aqueous media at low temperature. The microcrystals were characterized by X-ray diffraction (XRD), including powder X-ray diffraction structural determination, field-emission scanning electron microscopy (FE-SEM), and micro-Raman/ultraviolet-visible (UV-vis) diffuse reflectance spectroscopy. To complement the experimental data, we present first-principles quantum-mechanical density functional theory (DFT) calculations. Using XRD data, Raman/UV-vis data, and the determined optical band gap, together with geometric optimization calculations, we confirmed the structure of this compound. β-Ag_2WO_4 has a hexagonal structure with a $P6_3/m$ space group. The building blocks of the lattice comprise two types of W–O clusters, [WO_4] and [WO_5], coordinated to four and five O atoms, respectively, and two types of Ag–O clusters, [AgO_6], and [AgO_5], linked to six and five O atoms, respectively. This type of fundamental study, combining multiple experimental methods and first-principles calculations, helps to obtain a basic understanding of the local structure and bonding in the material.

Received 25th September 2015,
Accepted 23rd November 2015

DOI: 10.1039/c5dt03754a

www.rsc.org/dalton

1 Introduction

One of the holy grails of modern chemists is to synthesize and characterize inorganic, thermodynamically unstable, or metastable materials with desirable properties that are not exhibited by stable crystalline phases of the same materials.[1–5] Silver tungstate (Ag_2WO_4) based materials have received special attention from the scientific community because of their many possible applications, as photoluminescent materials, antibacterial agents, gas sensors, and photocatalysts.[6–21] Skarstad and Geller,[22] using the precipitation method, have discovered the existence of two phases of silver tungstate crystals (α- and β-Ag_2WO_4) but reported on crystallographic investigations of only α-Ag_2WO_4, which is the more stable of the two at high temperature. According to Mckechnie *et al.*,[23] β-Ag_2WO_4 crystals are obtained only at low temperatures (0–5 °C) when the pH is 8–10. Moreover, using powder X-ray diffraction (XRD), they verified that both α and β crystalline phases occur when the pH value is less than 8 at room temperature and below.

Further research by van den Berg and Juffermans[24] revealed the existence of polymorphism and the presence of three phases: α-Ag_2WO_4 (orthorhombic), β-Ag_2WO_4 (hexagonal), and γ-Ag_2WO_4 (cubic). The α phase is the thermodynamically stable phase among the three polymorphs,[24] and we have very recently reported on its local structure as well as on the photoluminescence properties of the material.[7] The Ag_2WO_4 lattices consist of a series of allotropic forms based on [WO_x] and [AgO_y] clusters as building blocks.

Metastable phases of materials have been reported to exhibit different physical and chemical properties from their thermodynamically stable counterparts. The prospect of novel properties and unique applications has fueled research in the preparation of metastable phases of materials. Because

[a]DQ-Universidade Federal de São Carlos, P.O. Box 676, CEP, 13565-905 São Carlos, São Paulo, Brazil
[b]Institute of Crystallography-CNR, Via G. Amendola 122/o, 70126 Bari, Italy
[c]Instituto Federal do Maranhão, PPG em Engenharia de Materiais, 65025-001, 65030-005 São Luís, MA, Brazil
[d]CDMF-Universidade Estadual Paulista, P.O. Box 355, 14801-907 Araraquara, SP, Brazil
[e]University Jaume I, Department of Analytical and Physical Chemistry, 12071 Castellon, Spain. E-mail: andres@qfa.uji.es
[f]DQ-GERATEC-Universidade Estadual do Piauí, João Cabral, N. 2231, P.O. Box 381, 64002-150 Teresina, PI, Brazil

†Electronic supplementary information (ESI) available: Theoretical active Raman modes. See DOI: 10.1039/c5dt03754a

α-Ag_2WO_4 is the thermodynamically stable phase, the unstable β and γ phases readily transform into the α form. Synthesis methods do not always lead to the most stable structure, with kinetic factors sometimes leading to an alternative phase. Reasonable control over the synthesis of β-Ag_2WO_4 crystals has proven to be a formidable challenge and has become the subject of intense research. Metastable β-Ag_2WO_4 was successfully prepared by precipitation methods using surfactant-assisted routes in which the proposed role of the surfactant is to prevent the β to α phase transformation.[20,25,26] Other free-surfactant routes, such as precipitation under conditions of pH = 4, which yielded metastable β-Ag_2WO_4 coexisting with a small amount of α-phase,[16] and pure β-Ag_2WO_4 synthesis at low temperature,[9] have also been reported. Ramezani *et al.*[27] synthesized β-Ag_2WO_4 nanoparticles using a simple electrochemical method.

In recent years, hexagonal β-Ag_2WO_4 has been investigated because of its photocatalytic and photoluminescence properties and the relationship of these properties with those of α-Ag_2WO_4 crystals.[11,12,14,19,20,28–30] However, to the best of our knowledge, the geometry and electronic structure of β-Ag_2WO_4 crystals have not been investigated either theoretically or experimentally. This encouraged us to investigate the geometry, cluster coordination, and electronic structure of metastable β-Ag_2WO_4 microcrystals synthesized here by the dropwise precipitation (DP) method in aqueous media at low temperature. We have characterized these microcrystals by different experimental techniques. We complemented these experiments with first-principles quantum-mechanical calculations using DFT in order to relate the results of XRD and Raman spectroscopy to the theoretical optical band gap and density of states (DOS) of metastable β-Ag_2WO_4.

The remainder of this paper is organized as follows. Section 2 describes the experimental procedure and computational details. Section 3 contains the results and discussion. Section 4 provides a summary of this study and concluding remarks.

2 Experimental and theoretical methods

2.1 General remarks

All experimental procedures were performed using deionized water and commercial reactants. Micro-Raman measurements were recorded using a LabRAM HR 800 mm model (Horiba, Jobin-Yvon, France). High-resolution Raman spectra in the range of 25 to 1000 cm^{-1} were recorded using a He–Ne laser (model CCD DU420AOE325) operating at 514.5 nm with an output power of 4 mW. A 50 μm lens was used to prevent sample overheating. UV-vis diffuse reflectance data were measured using a Cary 5G spectrophotometer (Varian, USA) in a diffuse reflection mode. All the experimental measurements were performed three times for each sample in order to ensure the reliability of the measurements. The shapes and sizes of the β-Ag_2WO_4 particles were observed with an Inspect F50 field-emission scanning electron microscope (FE-SEM) (FEI Company, Hillsboro, OR) operated between 5 and 20 kV.

2.2 Synthesis of β-Ag_2WO_4

A solution of 4 mmol of silver nitrate ($AgNO_3$; 99.8% purity, Sigma-Aldrich) in 50 mL of water was cooled to 15 °C and added dropwise at 2 mL min^{-1} to a solution of 2 mmol of tungstate sodium dihydrate ($Na_2WO_4{\cdot}2H_2O$; 99.0% purity, Sigma-Aldrich) dissolved in 50 mL of deionized water at 15 °C. The reaction mixture was continuously stirred for one hour. The resulting solid phase was separated from the solution by centrifugation (7000 rpm for five minutes). The solid was then washed with water (50 mL, 6 times) and acetone (50 mL, once) to remove any remaining Na^+ and NO_3^- ions. Each time, the solid was separated from the liquid using a centrifuge. Finally, the solid was dried at room temperature under vacuum in a desiccator containing blue silica gel.

2.3 X-ray diffraction studies

The β-Ag_2WO_4 crystals were structurally characterized by powder XRD using a LabX XRD-6000 diffractometer (Shimadzu, Japan) with Cu-Kα radiation (λ = 1.5406 Å). A 2θ-scan was performed from 10° to 70° with a scanning velocity of 2° min^{-1} and from 5° to 110° with a scanning velocity of 1° min^{-1}. The step size was 0.02°. The diffraction peaks were indexed in the hexagonal system using the N-TREOR09 indexing tool.[31] Crystal structure determination was carried out using EXPO2013,[32] a software package for phasing crystal structures from powder diffraction patterns.

2.4 Optical band gap

The optical band gap energy (E_{gap}) was calculated by the method proposed by Kubelka and Munk.[33] This methodology is well known, and it is described in several papers in the literature.[34–38] We calculated the E_{gap} values of our metastable β-Ag_2WO_4 microcrystals for the allowed indirect electronic transitions.

2.5 Computational details

Electronic structure calculations for the metastable crystalline β-Ag_2WO_4 structure were performed with the CRYSTAL14 software package.[39] W atoms were described by a large-core effective core potential, derived by Hay and Wadt, and modified by Cora *et al.*[40] Ag and O atoms were described using HAYWSC-311d31G and 6-31d1G basis sets, respectively, which were obtained from the Crystal web site.[41] Becke's three-parameter hybrid non-local exchange functional[42] was used in combination with a Lee–Yang–Parr gradient-corrected correlation functional (B3LYP).[43] The diagonalization of the Fock matrix was performed using an adequate number of *k*-points grids in the reciprocal-space. The thresholds controlling the accuracy of the calculation of the Coulomb and exchange integrals were set to 1×10^{-8} and 1×10^{-14}, and the percent of Fock/Kohn–Sham matrix mixing was set to 40 (IPMIX keyword).[39] The lattice parameters and the internal atomic coordinates were fully optimized until all force components

were less than 10^{-6} eV Å^{-2}. Raman vibrational modes and their corresponding frequencies were calculated using numerical second derivatives of total energies as implemented in the CRYSTAL14 package.[39] The band structure of bulk β-Ag_2WO_4 was constructed along the appropriate high-symmetry directions of the corresponding irreducible Brillouin zone.

3 Results and discussion

Metastable β-Ag_2WO_4 crystals were synthesized by a simple DP method in aqueous media at 15 °C in deionized water. The product was a light gray microcrystalline powder. The morphology of the metastable phase was observed by FE-SEM. The particles exhibited an elongated plate-like shape, as shown in Fig. 1, with a polydispersed distribution for both height and width. The images also show that the particles have cavities on their surfaces.

Four hundred and seventy crystals with good surface contours were selected for statistical analysis. The particles have a large size range with a length between 1.1 and 38.9 μm (see Fig. 2). However, about 90% of the particles have a length between 1.0 and 15.0 μm, and the average size, given by the peak of the normal curve in Fig. 2, is 8.1 μm. A comparative analysis of the images reveals that this synthesis method produces β-Ag_2WO_4 crystals that are larger than the previously reported α-Ag_2WO_4 crystals.[7] A possible explanation for this is that the higher symmetry of the hexagonal β-phase promotes a major growth rate.

Fig. 3 shows the XRD pattern of the metastable β-Ag_2WO_4 phase. The sharp and well-defined diffraction peaks indicate a high degree of structural order and crystallinity at long range of lattice. All the diffraction peaks are in good agreement with those reported for β-Ag_2WO_4 in the database of the Joint

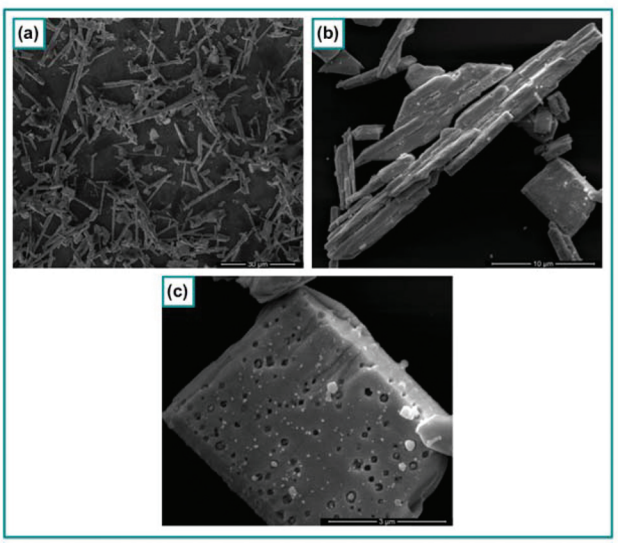

Fig. 1 FE-SEM images for β-Ag_2WO_4 microcrystals: (a) low magnification, (b) intermediate magnification and (c) high magnification.

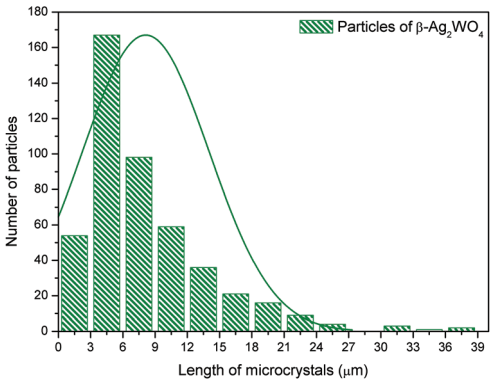

Fig. 2 Average size distribution of β-Ag_2WO_4 microcrystals.

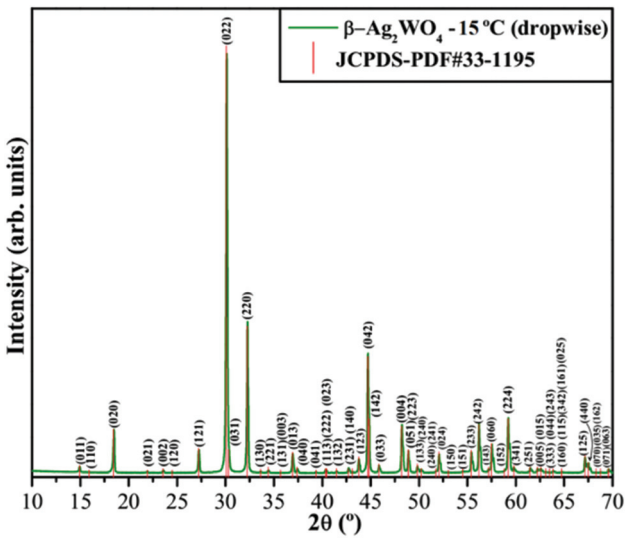

Fig. 3 XRD patterns of β-Ag_2WO_4 microcrystals.

Committee on Powder Diffraction Standards (JCPDS, card no. 33-1195) (see Fig. 3).[9,24,25] With the powder XRD pattern and the chemical formula as starting points, the *ab initio* structure calculation was carried out using the EXPO2013 software package.[32] First, the hexagonal cell parameters (a = 11.08904 Å, b = 11.08904 Å, c = 7.54062 Å, α = 90°, β = 90°, γ = 120°) were determined by the application of the N-TREOR09 indexing tool.[31] The unit cell volume indicated the presence of eight molecules per unit cell (Z = 8). The automatic space group identification procedure[44] suggested that the most probable space groups are $P6_3/m$, $P6_3$ (according to van den Berg and Juffermans[24]), and $P6_322$. The space group $P6_3/m$ was then selected for structure determination. Direct methods[45] were applied to extract atom positions. The positions of the heavy atoms (Ag and W) were quite easily determined. W atoms are at special positions 6h and 2a, while one Ag atom lies at special position 4f and the other at general position 12i. The O atom positions were determined using Fourier difference maps and the least-squares Fourier recycling technique. One

Table 1 Lattice parameters, unit-cell volume and internal atomic coordinates for β-Ag_2WO_4 from EXPO2013 and DFT calculations

β-Ag_2WO_4 (EXPO2013)			
	Lattice parameters		
	$a = b$ (Å)	c (Å)	Cell volume (Å^3)
	11.0890(4)	7.5406(2)	803.01(8)
	Internal atomic coordinates		
Atoms	x	y	z
W1	0.5124	0.0276	0.25
W2	0.0	0.0	0.25
Ag1	0.3333	0.6667	0.0463
Ag2	0.1597	0.8351	0.0269
O4	0.2052	0.0253	0.25
O5	0.3474	0.8656	0.25
O8	0.0	0.0	0.0
O10	0.6411	0.1130	0.4442
O11	0.6535	0.9829	0.25
β-Ag_2WO_4 (DFT)			
	Lattice parameters		
	$a = b$ (Å)	c (Å)	Cell volume (Å^3)
	11.0847	7.7099	820.417
	Internal atomic coordinates		
Atoms	x	y	z
W1	0.5262	0.02501	0.25
W2	0.0	0.0	0.25
Ag1	0.3333	0.6667	0.04192
Ag2	0.13607	0.8121	0.00828
O4	0.15540	0.16558	0.25
O5	0.3729	0.03577	0.25
O8	0.0	0.0	0.0
O10	0.62658	0.11366	0.43034
O11	0.5026	0.8559	0.25

O atom is at general position 12i, two are at special position 6h, and one is at special position 2b.[46]

Table 1 lists the crystal lattice parameters and the atomic positions of all atoms obtained with EXPO2013. The present procedure of synthesizing the metastable β-phase, performed with a simple DP method in aqueous media at low temperature and without the presence of surfactants, appears to be a highly efficient alternative to previously described procedures.[9,20,25–27]

At this point, we performed geometric optimization of the crystal structure using theoretical DFT calculations with the experimental crystallographic parameters. These optimized parameters are listed in Table 1. An analysis and comparison of both results, the EXPO2013 structure determination and the DFT calculations, show variations in the atomic positions of O associated with the fact that these atoms do not occupy fixed positions in the hexagonal structure; large variations in the position of O atoms in the lattice are found.

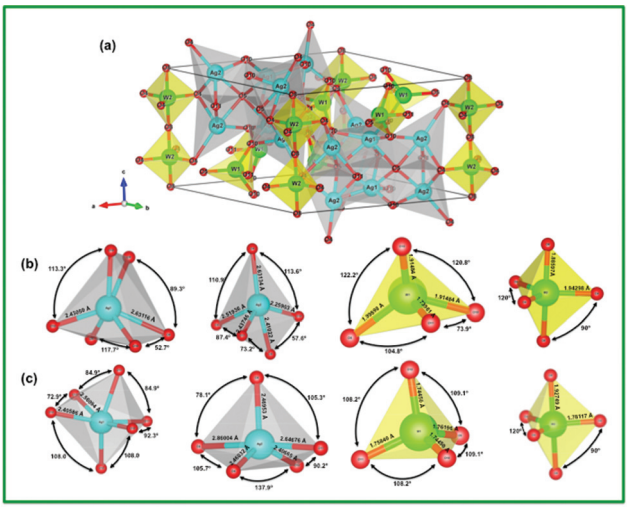

Fig. 4 (a) Polyhedral representation of the hexagonal β-Ag_2WO_4 unit cells, and different clusters of [AgO_y] (y = 6, or 5) and [WO_z] (z = 4, or 5); (b) experimental data and (c) theoretical calculations. The Ag, W, and O atoms are shown in light blue, green, and red, respectively.

To interpret the data we assume that these disagreements in the atomic positions of O atoms can be attributed to the nature of the starting sample (polycrystalline powder or single crystal). Although single-crystal data are essential to the refinement of crystal-structure models, we believe that the formation of different distortions in the cluster coordinations, [AgO_y] (y = 6, or 5) and [WO_z] (z = 4, 5), can lead to the formation of different types of distortions in the Ag–O and/or W–O bonds as well as O–Ag–O and/or O–W–O bond angles. Subsequently, the positions of O, W, and Ag atoms are variable. A similar phenomenon has been previously found for the α-Ag_2WO_4 phase.[7]

To clarify this point, we present in Fig. 4(a) a polyhedral representation of the unit cell of hexagonal β-Ag_2WO_4. The clusters of [AgO_y] (y = 6, 5) and [WO_z] (z = 4, 5) are clearly seen as the building blocks of the structure. This unit cell was modeled using the software package Visualization System for Electronic and Structural Analysis (VESTA, version 3.2.1).[47,48] Using lattice parameters and internal atomic positions obtained from the structural determination with the EXPO2013 software, we present the geometry of the different clusters in Fig. 4(b). The cluster geometries determined by DFT calculations are shown in Fig. 4(c).

Analysis of the results shows that there are two kinds of W atoms (W1 and W2) and two kinds of Ag atoms (Ag1 and Ag2). W1 atoms are coordinated to four O atoms forming distorted tetrahedral [WO_4] clusters, while the W2 atoms are at the center of distorted trigonal bipyramidal [WO_5] clusters. Ag1 atoms are coordinated to six O atoms forming distorted octahedral [AgO_6] clusters, while the Ag2 atoms belong to distorted trigonal bipyramidal [AgO_5] clusters.

The EXPO2013 analysis and the DFT calculations provide a consistent picture of the presence of several types of well-

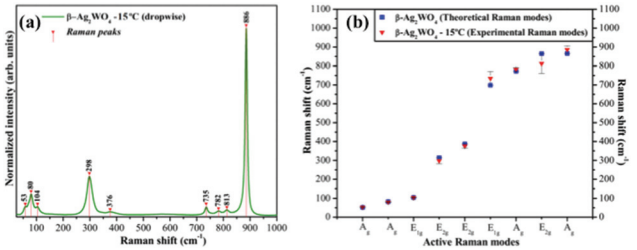

Fig. 5 (a) Micro-Raman spectrum of β-Ag_2WO_4 microcrystals, and (b) comparison between the relative positions of the theoretical and experimental Raman-active modes.

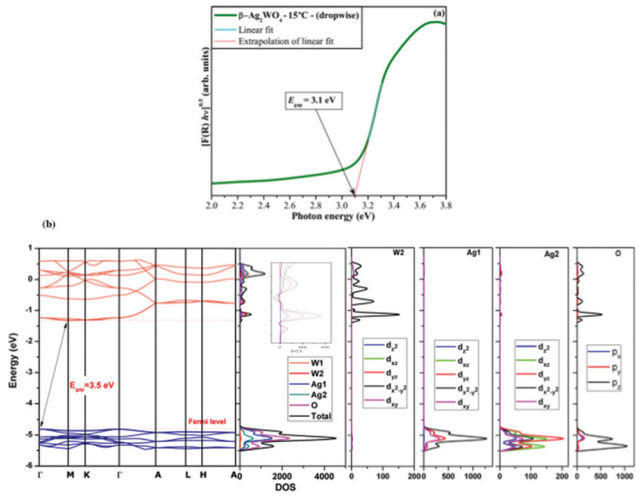

Fig. 6 (a) UV-Vis spectrum of β-Ag_2WO_4 microcrystals, and (b) band structure and DOS for β-Ag_2WO_4.

ordered clusters characterized by the metal–oxygen coordination. However, there are differences between the results of the EXPO2013 structural determination and the results of the DFT-optimized geometry. A comparison between the Ag–O and W–O distances, and in particular, the O–Ag–O and O–W–O bond angles (see Fig. 4(b) and (c)) shows the presence of more regular trigonal bipyramidal [WO_5] clusters and tetrahedral [WO_4] clusters in the DFT-determined geometry. This finding explains why assignment of the atomic positions of O atoms is difficult; subtle atomic rearrangements occur.

The XRD experiments provided only average structures. Better understanding of the material properties requires more detailed information on local structures and cell parameters. In other words, if there exists partial order in the distribution of Ag and W atoms, crystal cells observed at the local level should be different from those determined by XRD experiments. Raman spectroscopy probes the full vibrational manifold of interest because it is sensitive to short-range structural order, *i.e.*, the local metal coordination. Consequently, we extended our systematic structural investigation with Raman spectroscopy and theoretical analysis of the vibrational modes. The micro-Raman spectrum of β-Ag_2WO_4 microcrystals is shown in Fig. 5(a).

As seen in Fig. 5(a), the micro-Raman spectrum revealed the presence of only nine Raman-active vibrational modes (A_g, E_{1g}, and E_{2g}). Other Raman-active modes were not detectable experimentally because of their low intensities. The strength and frequencies of Raman vibrational modes were calculated and compared with the experimentally determined values as a way to validate the DFT-optimized structure. Calculated Raman-active vibrational modes are shown in Table S1 of the ESI,† while the relative positions of the theoretical and experimental Raman-active modes are depicted in Fig. 5(b), including labels for main modes (A_g, E_{1g}, and E_{2g}). Good agreement between experimental and calculated Raman-active modes is found, and these results allow us to confirm the structure of β-Ag_2WO_4 achieved in this study.

The theoretical Raman-active modes (collected in Table S1, ESI†) can be organized into three different groups. The first group is composed of modes in the frequency range of 40 to 205 cm^{-1}. These modes are separated by a phonon gap of nearly 65 cm^{-1} from internal symmetric and asymmetric bending modes of the tetrahedral [WO_4] clusters and trigonal-bipyramidal [WO_5]. In the second group, at high frequencies, there are nine modes corresponding to [← O ← W → O →] symmetric and/or [← O –W → / ← O–W →] asymmetric stretching modes of O–W–O and O–W structural units. The third group, separated from the second one by a phonon gap of 175 cm^{-1}, is dominated by a strong A_g mode at 772 cm^{-1}, related to the symmetric stretching of the [WO_5] units, and strong A_g and E_{2g} bands at 865 cm^{-1} due to modes derived from the symmetric-stretching vibration of the tetrahedral [WO_4] clusters. It is important to note that no vibrational modes associated with clusters involving Ag atoms are found in the experimental Raman spectrum.

As mentioned above, the optical band-gap energy (E_{gap}) was calculated with the method proposed by Kubelka and Munk.[33] When $F(R_\infty)$ is plotted against $h\nu$, where h is Planck's constant and ν is the frequency, the value of E_{gap} is found to be 3.1 eV. This gap can be associated with the presence of medium-range structural defects (local bond distortions), intrinsic surface states, and interfaces, which yield localized electronic levels within the forbidden band gap between the valence band (VB) and conduction band (CB) of metastable β-Ag_2WO_4 microcrystals.

The UV-vis diffuse reflectance spectrum for metastable β-Ag_2WO_4 microcrystals is shown in Fig. 6(a), and the calculated electronic band structure and DOS are shown in 6(b). The exponential optical-absorption edge and the optical band gap energy are controlled by the degree of structural order–disorder in the lattice (Fig. 6(a)).

Calculations yield an indirect band gap value of 3.5 eV from Γ to M points in the Brillouin zone, and for a simplified description, this difference can be mainly attributed to the distortions of both [AgO_y] (y = 6, 5) and [WO_z] (z = 4, 5) clusters at short and medium-range. An analysis of the site-projected DOS for specific atoms shows that the CB is mainly derived

from W2 atoms, which form [WO_5] clusters, while W1 atoms [WO_4] have a negligible contribution. The VB is mainly formed by O and Ag1 electronic states, with a minor contribution from the Ag2 atoms that form [AgO_5] clusters. Analysis of the DOS projected on orbitals shows that the top of the VB is mainly formed by hybridization between Ag 4d and O 2p orbitals, while the bottom of the CB is mainly formed by hybridization between W 5d and O 2p orbitals. For W and Ag1 metals, $4d_{x^2-y^2}$ states are the major contributors, while for Ag2, the VB maximum is derived mostly from $4d_{yz}$ states. The main role in changing the band gap belongs to the shift of the bottom of the CB, the position of which depends on the β-Ag_2WO_4 crystalline form. The location of the bottom of the CB is governed by the charge transfer from the W2 atom to the O atom in the [WO_5] clusters, which depends strongly on the W atom coordination symmetries.

Finally, it is worth mentioning that the relative positions of O, W, and Ag atoms in the β-Ag_2WO_4 lattice are variable, causing changes in the corresponding bond lengths and bond angles and distortions in the [WO_4], [WO_5], [AgO_6], and [AgO_5] clusters that lead to variations in the electronic density and energy band structure. This behavior has been observed previously for the α-Ag_2WO_4 lattice.[7,15]

4 Conclusions

Metastable phases of materials have been reported to exhibit different physical and chemical properties from their thermodynamically stable counterparts. Research on the preparation of metastable phases with novel properties has attracted great attention because of their variety of potential applications. This study not only provides new information on the geometry, cluster coordination, and electronic structure of metastable β-Ag_2WO_4 microcrystals but also illustrates the potential of the joint use of experimental techniques and first-principles DFT calculations. This combination led us to develop a systematic procedure to study the structure and electronic DOS of β-Ag_2WO_4. We find that it exhibits a hexagonal structure, formed by two types of W–O clusters, [WO_4] and [WO_5], and two types of Ag–O clusters, [AgO_6] and [AgO_5]. These clusters act as building blocks for the β-Ag_2WO_4 lattice. Features in the Raman spectra were identified by comparison with calculated vibrational frequencies, and this confirmed the predicted structure of this compound. The UV-vis spectrum indicated that β-Ag_2WO_4 microcrystals have an indirect band gap with a value of E_{gap} = 3.1 eV.

It is expected that this practical and controllable synthesis method may inspire the synthesis of metastable phases of other complex metal oxides. The present results provide a convenient example of a "complex modeling paradigm", introduced by Billinge and Levin.[49] The coupling of multiple experimental methods and first principle calculations result in a self-consistent computational framework that is essential for understanding the structure and properties of β-Ag_2WO_4. Furthermore, it opens the door to analyze transformations in this material and potential technological applications. Future investigations will be conducted to confirm the real potential of β-Ag_2WO_4. These investigations will offer new possibilities for creating complex functional materials that can be optimized for a large number of emerging applications in, for example, biology, catalysis, and photoluminescence. Further structural studies, such as those involving neutron diffraction, will be required to confirm the structure proposed in this study. The information in this paper will provide valuable insight not only into more investigations into β-Ag_2WO_4 but also into potential patterns in the complex behavior of this material system.

Acknowledgements

The authors acknowledge the financial support of agencies: CAPES (PNPD – 1268069), FAPESP (2013/07296-2; 2013/26671-9), CNPq (304531/2013-8), Generalitat Valenciana for *PrometeoII*/2014/022 and ACOMP/2014/270, Ministerio de Economia y Competitividad, project CTQ2012-36253-C03-02, and to the Spanish Brazilian program (PHB2009-0065-PC). We also acknowledge the Servei Informática, Universitat Jaume I for a generous allotment of computer time.

Notes and references

1 T. Nishimura, S. Hosokawa, Y. Masuda, K. Wada and M. Inoue, *J. Solid State Chem.*, 2013, **197**, 402–407.
2 R. Esmilaire, M. Beaudhuin, P. Hermet, N. Frety, D. Ravot and R. Viennois, *Mater. Lett.*, 2015, **138**, 222–224.
3 Y. Lu, Y. Zhao, J. Zhao, Y. Song, Z. Huang, F. Gao, N. Li and Y. Li, *Cryst. Growth Des.*, 2015, **15**, 1031–1042.
4 T. Jaron, W. Wegner, K. J. Fijalkowski, P. J. Leszczynski and W. Grochala, *Chem. – Eur. J.*, 2015, **21**, 5689–5692.
5 A. Zakutayev, A. J. Allen, X. Zhang, J. Vidal, Z. Cui, S. Lany, M. Yang, F. J. DiSalvo and D. S. Ginley, *Chem. Mater.*, 2014, **26**, 4970–4977.
6 X. J. Cui, S. H. Yu, L. L. Li, L. Biao, H. B. Li, M. S. Mo and X. M. Liu, *Chem. – Eur. J.*, 2004, **10**, 218–223.
7 L. S. Cavalcante, M. A. P. Almeida, W. Avansi, R. L. Tranquilin, E. Longo, N. C. Batista, V. R. Mastelaro and M. S. Li, *Inorg. Chem.*, 2012, **51**, 10675–10687.
8 E. Longo, L. S. Cavalcante, D. P. Volanti, A. F. Gouveia, V. M. Longo, J. A. Varela, M. O. Orlandi and J. Andres, *Sci. Rep.*, 2013, **3**, 1676.
9 H. Chen and Y. Xu, *Appl. Surf. Sci.*, 2014, **319**, 319–323.
10 D. P. Dutta, A. Singh, A. Ballal and A. K. Tyagi, *Eur. J. Inorg. Chem.*, 2014, 5724–5732, DOI: 10.1002/ejic.201402612.
11 J. Tang and J. Ye, *J. Mater. Chem.*, 2005, **15**, 4246–4251.
12 R. Zhang, H. Cui, X. Yang, H. Tang, H. Liu and Y. Li, *Micro Nano Lett.*, 2012, **7**, 1285–1288.
13 L. Pan, L. Li and Q. Zhu, *J. Sol–Gel Sci. Technol.*, 2013, **67**, 573–579.

14 E. Longo, D. P. Volanti, V. M. Longo, L. Gracia, I. C. Nogueira, M. A. P. Almeida, A. N. Pinheiro, M. M. Ferrer, L. S. Cavalcante and J. Andres, *J. Phys. Chem. C*, 2014, **118**, 1229–1239.
15 J. Andrés, L. Gracia, P. Gonzalez-Navarrete, V. M. Longo, W. A. Jr, D. P. Volanti, M. M. Ferrer, P. S. Lemos, F. A. L. Porta, A. C. Hernandes and E. Longo, *Sci. Rep.*, 2014, **5**, 5391.
16 Y. V. B. De Santana, J. E. Cardoso Gomes, L. Matos, G. H. Cruvinel, A. Perrin, C. Perrin, J. Andres, J. A. Varela and E. Longo, *Nanomater. Nanotechnol.*, 2014, **4**, 10.
17 L. F. da Silva, A. C. Catto, W. Avansi Jr., L. S. Cavalcante, J. Andres, K. Aguir, V. R. Mastelaro and E. Longo, *Nanoscale*, 2014, **6**, 4058–4062.
18 V. M. Longo, C. C. D. Foggi, M. M. Ferrer, A. F. Gouveia, R. S. André, W. Avansi, C. E. Vergani, A. L. Machado, J. Andrés, L. S. Cavalcante, A. C. Hernandes and E. Longo, *J. Phys. Chem. A*, 2014, **118**, 5769–5778.
19 W. D. S. Pereira, J. Andres, L. Gracia, M. A. San-Miguel, E. Z. da Silva, E. Longo and V. M. Longo, *Phys. Chem. Chem. Phys.*, 2015, **17**, 5352–5359.
20 X.-Y. Zhang, J.-D. Wang, J.-K. Liu, X.-H. Yang and Y. Lu, *CrystEngComm*, 2015, **17**, 1129–1138.
21 M. Vafaeezadeh and M. M. Hashemi, *RSC Adv.*, 2015, **5**, 31298–31302.
22 P. M. Skarstad and S. Geller, *Mater. Res. Bull.*, 1975, **10**, 791–799.
23 J. S. McKechnie, L. D. S. Turner, C. A. Vincent, F. Bonino, M. Lazzari and B. Rivolta, *J. Inorg. Nucl. Chem.*, 1979, **41**, 177–179.
24 A. J. van den Berg and C. A. H. Juffermans, *J. Appl. Crystallogr.*, 1982, **15**, 114–116.
25 X. Wang, C. Fu, P. Wang, H. Yu and J. Yu, *Nanotechnology*, 2013, **24**, 165602–165609.
26 J. Li, C. Yu, C. Zheng, A. Etogo, Y. Xie, Y. Zhong and Y. Hu, *Mater. Res. Bull.*, 2015, **61**, 315–320.
27 M. Ramezani, S. M. Pourmortazavi, M. Sadeghpur, A. Yazdani and I. Kohsari, *J. Mater. Sci.: Mater. Electron.*, 2015, **26**, 3861–3867.
28 J. Zhu, H. Fan, J. Sun and S. Ai, *Sep. Purif. Technol.*, 2013, **120**, 134–140.
29 X. Liu, J. Hu, J. Li, Y. Hu, Y. Shao, H. Yang, G. Tong and H. Qian, *Mater. Lett.*, 2013, **91**, 129–132.
30 A. Sreedevi, K. P. Priyanka, K. K. Babitha, N. Aloysius Sabu, T. S. Anu and T. Varghese, *Indian J. Phys.*, 2015, **89**, 889–896.
31 A. Altomare, G. Campi, C. Cuocci, L. Eriksson, C. Giacovazzo, A. Moliterni, R. Rizzi and P.-E. Werner, *J. Appl. Crystallogr.*, 2009, **42**, 768–775.
32 A. Altomare, C. Cuocci, C. Giacovazzo, A. Moliterni, R. Rizzi, N. Corriero and A. Falcicchio, *J. Appl. Crystallogr.*, 2013, **46**, 1231–1235.
33 P. Kubelka and F. Munk, *Zeit. Fur. Tech. Physik*, 1931, **12**, 593–601.
34 L. S. Cavalcante, E. Moraes, M. A. P. Almeida, C. J. Dalmaschio, N. C. Batista, J. A. Varela, E. Longo, M. S. Li, J. Andres and A. Beltran, *Polyhedron*, 2013, **54**, 13–25.
35 T. Badapanda, S. Sarangi, B. Behera, P. K. Sahoo, S. Anwar, T. P. Sinha, G. E. Luz Jr., E. Longo and L. S. Cavalcante, *Curr. Appl. Phys.*, 2014, **14**, 708–715.
36 A. F. Gouveia, J. C. Sczancoski, M. M. Ferrer, A. S. Lima, M. R. M. C. Santos, M. S. Li, R. S. Santos, E. Longo and L. S. Cavalcante, *Inorg. Chem.*, 2014, **53**, 5589–5599.
37 C. W. Raubach, A. F. Gouveia, Y. V. B. de Santana, J. A. Varela, M. M. Ferrer, M. S. Li and E. Longo, *J. Mater. Chem. C*, 2014, **2**, 2743–2750.
38 R. A. Roca, J. C. Sczancoski, I. C. Nogueira, M. T. Fabbro, H. C. Alves, L. Gracia, L. P. S. Santos, C. P. de Sousa, J. Andres, G. E. Luz Jr., E. Longo and L. S. Cavalcante, *Catal. Sci. Technol.*, 2015, **5**, 4091–4107.
39 R. Dovesi, V. R. Saunders, C. Roetti, R. Orlando, C. M. Zicovich-Wilson, F. Pascale, B. Civalleri, K. Doll, N. M. Harrison, I. J. Bush, P. D'Arco, M. Llunel, M. Causà and Y. Noël, *CRYSTAL14 User's Manual*, Theoretical Chemistry Group, University of Turin, Italy, 2014.
40 F. Cora, A. Patel, N. M. Harrison, R. Dovesi and C. R. A. Catlow, *J. Am. Chem. Soc.*, 1996, **118**, 12174–12182.
41 http://www.crystal.unito.it/basis-sets.php.
42 A. D. Becke, *J. Chem. Phys.*, 1993, **98**, 5648–5652.
43 C. T. Lee, W. T. Yang and R. G. Parr, *Phys. Rev. B: Condens. Matter*, 1988, **37**, 785–789.
44 A. Altomare, C. Cuocci, A. Moliterni and R. Rizzi, *J. Appl. Crystallogr.*, 2013, **46**, 476–482.
45 A. Altomare, C. Cuocci, C. Giacovazzo, A. Moliterni and R. Rizzi, *J. Appl. Crystallogr.*, 2008, **41**, 592–599.
46 A. Altomare, C. Cuocci, C. Giacovazzo, A. G. G. Moliterni and R. Rizzi, *J. Appl. Crystallogr.*, 2006, **39**, 558–562.
47 K. Momma and F. Izumi, *J. Appl. Crystallogr.*, 2008, **41**, 653–658.
48 K. Momma and F. Izumi, *J. Appl. Crystallogr.*, 2011, **44**, 1272–1276.
49 S. J. L. Billinge and I. Levin, *Science*, 2007, **316**, 561–565.